Revision 1

Quantification of Water in Majoritic Garnet

Sylvia-Monique Thomas[1], Kathryn Wilson[1], Monika Koch-Müller[2], Erik H. Hauri[3], Catherine McCammon[4], Steven D. Jacobsen[5], John Lazarz[5], Dieter Rhede[2], Minghua Ren[1], Neal Blair[5], Stephan Lenz[2]

[1]Department of Geoscience, University of Nevada Las Vegas, Las Vegas, NV 89154, USA

(sylvia-monique.thomas@unlv.edu)

[2]Helmholtz-Zentrum Potsdam, Deutsches GeoForschungsZentrum (GFZ), 14473 Potsdam, Germany

[3]Department of Terrestrial Magnetism, Carnegie Institution of Washington, Washington, DC 20015, USA

[4]Bayerisches Geoinstitut, Universität Bayreuth, 95440 Bayreuth, Germany

[5]Department of Earth and Planetary Sciences, Evanston, IL 60208, USA

Abstract

Majoritic garnet, characterized by an excess of silicon (>3 Si per formula unit), is considered one of the major phases of the Earth's transition zone from 410-660 km depth. Quantifying the H_2O content of nominally anhydrous mantle minerals is necessary to evaluate their water storage capacity from experiments and modeling the Earth's deep water cycle. We present mineral-specific infrared absorption coefficients for the purpose of quantifying the amount of water incorporated into majorite as hydroxyl point defects. A suite of majoritic garnet samples with varying proportions of Si, Fe, Al, Cr and H_2O was synthesized at conditions of 18-19 GPa and 1500-1800°C. Single-crystals were characterized using X-ray diffraction, electron microprobe analysis, secondary Ion Mass spectrometry (SIMS), IR, Raman and Mössbauer spectroscopy. We utilize SIMS and Raman spectroscopy in combination with IR spectroscopy to provide IR absorption coefficients for water in majoritic garnets with the general mineral formula $(Mg,Fe)_3(Si,Mg,Fe,Al,Cr)_2[SiO_4]_3$. The IR absorption coefficient for majoritic garnet in the OH stretching region is frequency-dependent and ranges from 10470 ± 3100 $Lmol^{-1}cm^{-2}$ to 23400 ± 2300 $Lmol^{-1}cm^{-2}$.

Keywords: IR spectroscopy, water in nominally anhydrous minerals, transition zone, integral molar absorption coefficient, SIMS, high pressure, Raman spectroscopy

Introduction

Majorite was first described by Smith and Mason (1970), who found a garnet with silicon excess (more than 3 silicon atoms per formula unit) in the Coorara meteorite. They further defined majorite as garnet solid solution with partial occupancy of the octahedral site by excess Si and Mg. The first terrestrial occurence was reported by Moore and Gurney in 1985, who discovered majorite inclusions in kimberlitic diamonds. Garnet, along with olivine and its high-pressure polymorphs wadsleyite and ringwoodite, are major components of the Earth's upper mantle and transition zone (Akaogi and Akimoto 1977; Anderson and Bass 1986; Irifune 1987).

With increasing depth the majoritic component of garnets increases towards the solid solution end member majorite (Maj), $Mg_3(Mg_1Si_1)Si_3O_{12}$ = $Mg_4Si_4O_{12}$, from small amounts in the upper mantle to significant amounts in the transition zone (e.g., Ringwood 1967; Ringwood and Major 1971; Kanzaki 1987; Irifune 1987; Gasparik 2002). Hence, majorite-pyrope ($Mg_4Si_4O_{12}$-$Mg_3Al_2Si_3O_{12}$) solid solutions are of high relevance for the Earth's transition zone, which can contain ≥ 40 % majorite depending on the petrological model considered (e.g., Ita and Stixrude 1992).

The incorporation of silicon into the octahedral site is facilitated by the above-mentioned majoritic component, which is a coupled substitution of tetravalent silicon and one divalent cation (M) in equal amounts replacing two trivalent cations ($2\ M^{3+} = Si^{4+} + M^{2+}$) (Ringwood 1967; Ringwood and Major 1971). This coupled substitution leads to the general crystal chemical formula $(Mg,Fe,Ca)_3(Si,Mg,Fe,Al,Cr)_2[SiO_4]_3$ and to a symmetry reduction; whereas Al-bearing majoritic garnet is cubic, endmember majorite crystallizes in tetragonal symmetry

due to ordering of Mg and Si on two distinct octahedral sites (Ringwood and Major 1967; Akaogi and Akamoto 1977; Hatch and Ghose 1989; Angel et al. 1989).

Majorite crystal structure, stability, compressibilities, elasticity, iron oxydation state and vibrational spectroscopy have been extensively studied in the past (e.g., Akaogi and Akimoto 1977; Hazen et al. 1994; Heinemann et al. 1997; Murakami et al. 2008; McCammon and Ross 2003; Hofmeister et al. 2004). In this work we focus on the incorporation of water into majoritic garnet. The presence of water, incorporated as OH through charge-coupled chemical substitutions into high-pressure silicates of the Earth's deep interior, may play a significant role in geophysical processes due to its influence on phase relations and melting behavior, conductivity, elasticity, viscosity and rheology (Smyth and Jacobsen 2006; Keppler and Smyth 2006; Hirschmann 2006). Theoretical studies and high pressure experiments indicate a significant water storage capacity of nominally anhydrous minerals composing the Earth's upper mantle, transition zone and lower mantle (e.g., Keppler and Smyth 2006). Recently, the first direct evidence for H_2O in the transition zone has been reported by Pearson et al. (2014), who found ~ 1.4 wt% H_2O dissolved in a ringwoodite diamond inclusion. Evidence for regional-scale hydration of the transition zone beneath North America was recently inferred from detection of dehydration melting below 600 km depth (Schmandt et al. 2014).

While for natural garnets of mantle origin a maximum water content of several hundreds of wt ppm H_2O has been reported (e.g., Beran et al. 1993; Beran and Libowitzky 2006), recent experiments found that synthetic majorite can store up to ~1300 wt ppm H_2O in its structure (Bolfan-Casanova et al. 2000; Katayama et al. 2003). Majorite is nominally anhydrous, i.e., water is incorporated as hydroxyl point groups through defect mechanisms. Such defect mechanisms can include the hydrogarnet substitution associated with tetrahedral sites, where SiO_4 is replaced by OH_4, but also vacancies in octahedral and dodecahedral sites or the substitution of silicon by trivalent aluminum and a proton in the tetrahedral sites

(Rossman and Aines 1991; Bolfan-Casanova 2000; Katayama 2003; McCammon et al. 2004; Mokherjee and Karato 2010).

To determine absolute water concentrations and to take advantage of the high sensitivity of IR spectroscopy for the detection of trace OH, mineral-specific absorption coefficients are essential. To date no mineral specific IR calibration constant has been reported for majorite. Several calibration attempts have been made for a wide variety of natural garnets with up to several hundreds of wt ppm H_2O using Nuclear Reaction Analyses, vacuum extraction and H_2 manometry (Rossman et al. 1988; Rossman 1990; Bell et al. 1995; Maldener et al. 2003). Bell et al. (1995) report an integral molar absorption coefficient of 6700 ± 670 $Lmol^{-1}cm^{-2}$ for a garnet megacryst of the Monastery kimberlite. Maldener et al. (2003) suggest the use of an average value of the 3470 $Lmol^{-1}cm^{-2}$ for pyrope-rich garnets, and 3630 ±1580 $Lmol^{-1}cm^{-2}$ for other compositions, based on the study of nine samples with different chemical compositions.

In this study we calculate absorption coefficients for a set of crystals in the majorite-pyrope solid-solution series using IR, Raman and SIMS measurements. We test the wavenumber-dependence of these absorption coefficients, compare them with literature data, and discuss OH incorporation mechanisms.

Methods

Syntheses and samples

Single-crystals of majoritic garnet with varying Si-, Fe-, Mg-, Al, Cr- and OH- contents were synthesized with and without water at 18 GPa and 1500°C or 1800 °C in the rotating multi-anvil press (for press specifications see Schmidt and Ulmer 2004; Deon et al. 2010) at GeoForschungsZentrum Potsdam (MA380 – 385, 337). The temperature was controlled using a W5%Re/W26%Re thermocouple. Note that we did not remove traces of adsorbed water from our dry run starting materials (MA380, MA382) as they might act as flux for the

growth of larger crystals. Pure oxide mixtures were loaded in Pt capsules for multi-anvil runs that were sealed by cold welding. Temperature cycling (final temperature ± 20 °C) was used during the first 30 minutes of the runs to enhance crystal growth. Samples Max3 and Max4 were synthesized at 19 GPa and 1800°C in a 1000-ton multi-anvil press from natural orthopyroxene at the Bayerisches Geoinstitut. Starting compositions and experimental conditions are listed in Table 1. After quenching, the Pt capsules were filed open for sample recovery. Isotropic single-crystals (50-500 μm in size) were used for analysis.

Microprobe analysis

For chemical analyses, individual grains of the majoritic garnets were polished, mounted in Indium and coated with carbon. Compositions were determined by wavelength-dispersive X-ray analysis (WDS) techniques using a JEOL JXA-8500F (HYPERPROBE) electron microprobe at the Deutsches GeoForschungsZentrum Potsdam (GFZ). The analytical conditions included an acceleration voltage of 15 kV, a beam current of 10 nA, and a focussed beam. The following natural and synthetic reference standards were used (respective element and peak counting time listed in brackets): wollastonite (for Ca; 20 s), almandine (for Fe; 30 s, and Al 30 s), pyrope (for Si; 30 s), MgO (for Mg; 20 s) and Cr_2O_3 (for Cr; 20 s). The background counting times were always set to half of the respective peak counting times. The CITZAF routine in the JEOL software, which is based on the F(rZ) method (Armstrong, 1995), was used for data processing.

X-ray diffraction

High-precision lattice parameters of majoritic garnets in this study were determined using single-crystal X-ray diffraction and the method of eight-position centering (King and Finger 1979; Angel and Finger 2011) on the Huber four-circle diffractometer at Northwestern University. For each sample, 30 reflections from 9 different (*hkl*) classes and with 2θ angles between 14 and 30 degrees. Unconstrained and symmetry constrained lattice parameters for each sample are provided in Table 2.

Mössbauer spectroscopy

Individual grains were mounted in clusters with approximately 300 μm overall diameter on mylar sheets using clear nail varnish. The grain mounts were centered inside holes ranging from 400 to 1000 μm diameter drilled in pieces of 25 μm thick Ta foil (absorbs 99% of 14.4 keV gamma rays). The dimensionless Mössbauer thickness estimated for the grain assemblages based on chemical compositions and physical thickness ranges from 1 to 4 and Mössbauer spectra were collected between 1 and 12 days.

Mössbauer spectra were recorded at room temperature (293 K) in transmission mode on a constant acceleration Mössbauer spectrometer with a nominal 370 MBq ^{57}Co high specific activity source in a 12 μm thick Rh matrix. The velocity scale was calibrated relative to 25 μm thick α-Fe foil using the positions certified for (former) National Bureau of Standards standard reference material no. 1541; line widths of 0.36 mm/s for the outer lines of α-Fe were obtained at room temperature. Mössbauer spectra were fitted using the program MossA (Prescher et al. 2012).

Mössbauer spectra were fitted to Lorentzian doublets according to current models in the literature (e.g., McCammon and Ross 2003). The usual constraints were applied to all doublets (equal component areas and widths) unless otherwise noted. Values for $Fe^{3+}/\Sigma Fe$ were calculated based on relative area ratios corrected for differences in recoil-free fraction, where the latter correction was based on the Debye model with assumed Mössbauer Debye temperatures for garnet of 340 and 400 K for Fe^{2+} and Fe^{3+}, respectively (Amthauer et al. 1976; De Grave & Van Alboom 1991).

IR spectroscopy

For IR spectroscopy, single-crystals were doubly polished with diamond lapping film using the 0.25 μm grade in the last step. For analysis the crystals were placed on a KBr plate. Unpolarized IR spectra of synthetic majoritic garnet were recorded from 1850 to 4000 cm^{-1} at

ambient conditions with a Bruker IFS 66v FTIR spectrometer, a Hyperion microscope, an InSb detector, a KBr beamsplitter, and a globar light source. Up to 1024 scans were taken with a resolution of 2 cm^{-1} through a 100 × 100 μm aperture. The sample thickness was determined using the eyepiece reticule and stage micrometer scale of the optical microscope. The final thickness varied from 30 to 40 μm depending on the specimen (cf. Table 3). A linear baseline correction in the integration limits between 3000 and 3750 cm^{-1} was applied for all our spectra. The integrated absorbances and area-weighted average (Libowitzky and Rossman 1996, 1997) of the peak positions were determined using PeakFit (Systat Software, Inc.). Quantitative measurements of single-crystals were obtained on randomly oriented sections. Polarized measurements are not needed for isotropic minerals, where the absorbance is linearly dependent on the species concentration and thickness of the sample. It is important to note that some authors use the sum of absorbances (total absorbance) in all three orthogonal directions of a crystal to calculate the absorption coefficient, others use only one-directional information. For our cubic majoritic garnets we use one-directional absorbance values derived from unpolarized spectra.

Raman spectroscopy

Single-crystals used in IR studies were characterized with confocal microRaman spectroscopy at Northwestern University. No additional sample preparation was required. All analyses were performed in backscattering geometry using an Andor Shamrock 0.3 m spectrograph (1800 grooves/mm grating) coupled to an Andor Newton EM-CCD camera, an Olympus optical microscope and a long working distance Mitutoyo 100x objective (LWD VIS, NA = 0.70, WD = 6.0 mm). The 458-nm line of a solid-state Melles Griot laser source with ~300 mW output power was used for sample excitation. Laser intensity at the sample was 18 mW. For all measurements a confocal aperture of 60 x 60 μm was used. For sample characterization spectra were acquired from 50 - 1300 cm^{-1}. Counting times were 20 s at 3 accumulations.

To independently quantify the water content in samples MA337 and MA380, Raman spectra were recorded at Helmholtz-Zentrum Deutsches GeoForschungsZentrum. The measurements were performed following the procedure described in Thomas et al. (2008, 2009). The 472-nm line of a Coherent Ar^+ Laser (Innova 70-3) with 300 mW output power, a LabRam HR800 UV-Vis spectrometer, a motorized XY-stage, an Olympus optical microscope, a long working distance 100x objective (LWD VIS, NA = 0.80, WD = 3.4 mm) and a Peltier-cooled CCD detector were used. Spectra in the frequency range from 2800 – 4000 cm^{-1} were taken with the 300 grooves/mm grating and a confocal setup (100 µm pinhole). After a linear baseline correction was performed, spectra were integrated between 3000 and 3750 cm^{-1}. Counting times were 10 s at 5 accumulations for MA337 and 50s at 10 accumulations for MA380. The SD-8.06% glass (cf. Thomas et al. 2008) was used as reference material. Mrosko et al. (2011) recommend for minerals with heavy cations a molar volume correction rather than a density correction for differences between sample and reference material (see reference for calculation details). For this reason a majoritic garnet correction factor of 0.788 was used for water quantification in samples MA337 and MA380.

Secondary-ion mass spectrometry

SIMS measurements of H in selected samples were performed on the Cameca NanoSIMS 50L scanning ion microprobe at the Carnegie Insitution of Washington. Polished single-crystals were mounted in indium. To flatten the surface and fill cavities around the crystals, the whole assembly was pressed with 4.9 t in a hydraulic press. The $^{16}OH^-$ signal was standardized using natural and synthetic minerals described in Koga et al. (2003) and Hauri et al. (2006): olivines SynFo100, SynFo68, GRR1012, KLV-23; orthopyroxenes KBH-1, India, Kenya, A288; garnets MON-9, ROM263-9, ROM263-25, ROM263-52; clinopyroxene PMR-53. We also used additional olivines and pyroxenes from the Monastery kimberlite that were studied by Bell et al. (2004): olivines ROM177, ROM250-13, ROM250-2; clinopyroxenes ROM271-10, ROM271-16, ROM271-21; orthopyroxene ROM273. Detailed analytical setup and methodology information is described in Hauri et al. (2006) and Koga et al. (2003).

Results

Sample characterization (Electron microprobe analyses, X-ray diffraction, Mössbauer spectroscopy)

Run products consisted of up to 500 µm sized single-crystals of majoritic garnet with significant amounts of Cr, Al, Fe and OH (Table 3). The ferric iron content was analyzed by Mössbauer spectroscopy and EELS (Lenz 2012) and ranged between 6 and 21 % depending on sample composition. Sample MA337, which is the only sample that was analyzed by EELS, has the highest Fe^{3+} concentration (Table 3). Even though two different technical approaches have been applied here, the determined ferric iron contents are expected to be comparable within uncertainties. In fact, Mrosko et al. (2013) used both tools at the same laboratories to determine the ferric iron concentration in ringwoodite and report values that are in good agreement. Mineral formulas are given in Table 3. With increasing silicon content, Al_2O_3 and FeO concentrations decrease, while the MgO content increases. Lattice constants and cell volume indicate the cubic crystal system for all samples (Table 2).

Mössbauer spectra are shown in Figure 1. The Mössbauer spectrum of sample MA380 was sufficiently well resolved that two doublets could be fitted to the spectrum without further constraints, yielding realistic values for all hyperfine parameters. When the Mössbauer spectra of samples MA382 and MA385 were fitted without further constraints, unrealistically large values of the widths of the Fe^{3+} doublets were obtained; hence these widths were constrained to 0.4 mm/s for these spectra. This value was chosen based on the width obtained for sample MA380 as well as literature values reported for a similar composition of majorite (McCammon and Ross 2003). A similar effect was observed in fitting the Mössbauer spectrum of sample MA384, except that an unrealistically low quadrupole splitting (QS) was obtained when the Fe^{3+} doublet width was constrained. In this case it was sufficient to constrain the QS value to 0.35 mm/s, while allowing the Fe^{3+} doublet width to vary. Mössbauer spectra of samples Max3 and Max4 were sufficiently resolved that no additional

constraints were required. Absorption near ~ 2 mm/s required the addition of a third doublet, which likely corresponds to octahedral Fe^{2+}. The consistency of hyperfine parameters in all of the fits were checked by plotting the centre shifts of all components against their quadrupole splitting and comparing values with the literature (McCammon and Ross 2003). All data are consistent with expected values within experimental error.

IR spectroscopy

Unpolarized IR spectra of majoritic garnet at room conditions are illustrated in Figure 2. Spectra are offset for clarity. All spectra are similar, though band intensities differ. The IR spectra are composed of broad absorption bands of OH stretching vibrations with maxima between ~3100 cm^{-1} and ~3630 cm^{-1} (Table 4). In general, bands at ~3580 cm^{-1} show strongest intensities. With increasing H_2O concentration OH band intensities at ~3630 cm^{-1} increase (cf. strongest band in MA384). Sample MA337, with the highest water content, shows an additional dominant OH band at ~3120 cm^{-1}.

Raman spectroscopy

Unpolarized Raman spectra of ~40 μm thick single-crystals of majoritic garnet are shown in Figure 3. The red spectrum is representative for the high-silica samples Max3 and Max4, whereas the black spectrum (MA384) is typical for the rest of the majoritic garnets (low-silica samples). Both spectra display a similar number of peaks and are characteristic for the cubic garnet structure with expected A_{1g} (360 cm^{-1}, 563 cm^{-1}, 928 cm^{-1}), E_g (868 cm^{-1}, 1064 cm^{-1}) and T_{2g} (211 cm^{-1}, 646 cm^{-1}) modes (McMillan et al. 1989). We follow the peak assignment in McMillan et al. (1989). The modes at ~360 cm^{-1} (A_{1g}), 868 cm^{-1} (E_g) and the strongest mode at 928 cm^{-1} (A_{1g}) are due to symmetric stretching vibrations of the SiO_4 tetrahedra. The mode at 1064 cm-1 (E_g) is associated with asymmetric stretching vibrations, and the peak at 563 cm^{-1} (A_{1g}) is caused by symmetric bending vibrations of the SiO_4 group. The spectrum representative for the two Si-rich samples looks very similar to the spectrum of a natural majorite found in a meteorite (Jeanloz, 1980) with a strong peak at 595 cm^{-1} and the 868 cm^{-1}

peak, which is strong in our Al-rich samples, being slightly shifted to 891 cm^{-1}. The small differences in peak positions and peak widths of the two spectra might be due to a slightly larger cell volume of the Si-richer compositions, and a higher cation disorder, respectively. According to McMillan et al. (1989) stiffening of the O-Si-O bending force constant during the substitution of Si by Al in octahedral might be responsible for the peak shift of the 563 cm^{-1} band.

Water contents and mineral-specific absorption coefficients

Sample water contents were determined by either confocal micro-Raman spectroscopy (MA337, MA380, Fig. 4) and/or secondary ion mass spectrometry (MA380-MA385, Max3, Max4). The H_2O concentration of the seven samples ranges from 126 to 2200 wt ppm (see Table 4). From water concentrations (c_{H2O}), peak-fitted integrated areas (A_i), samples thickness (d) and density (ρ), mineral-specific absorption coefficients (Table 1) were calculated using the Beer-Lambert law, $\varepsilon = (A_i \times 1.8) / (d \times \rho \times c_{H2O})$, with d in cm and c_{H2O} in wt%. Note that we use one-directional absorbance information (A_i) for our calculations, not the total absorbance from all three orthogonal directions of a crystal. For majoritic garnet absorption coefficients ranging from 10470 ± 3100 $Lmol^{-1}cm^{-2}$ to 23400 ± 2300 $Lmol^{-1}cm^{-2}$ were determined. The relative error of absorption coefficients is mainly determined by the error of the water concentration from all analyses (7% relative uncertainty from SIMS, ~20% standard deviation from Raman spectroscopy), sample thickness, density, the surface quality of the samples, and spectral fits. From Gaussian error propagation of relative errors from peak-fitted integrated areas (2%), sample density (2%), sample thickness (2%) and water content (~10%), we estimate the relative error of the absorption coefficient to be 11%.

Discussion

Whereas water contents determined for the majority of our synthetic majoritic garnets are consistent with literature data, we report a higher H_2O concentration of 2200 wt ppm in

MA337. Prior reported values typically range from 1 up to some hundreds of wt ppm H_2O in natural specimens of mantle origin, but extend to ~1300 wt ppm H_2O in synthetic samples (Lu and Keppler 1997; Withers et al. 1998; Bolfan-Casanova et al. 2000; Katayama et al. 2003; Mookherjee and Karato 2010). A spectrum shown in figure 2 of the study of Bolfan-Casanova et al. (2000) implies even ~2000 wt ppm H_2O for cubic garnet (pyrope) when compared with 677 wt ppm H_2O in Al-free majorite.

Pressure, temperature, water fugacity and chemical impurities can increase the water solubility in nominally anhydrous minerals. This has been observed for a range of minerals in the past, e.g., for stishovite (Pawley et al., 1993) and olivine (Kohlstedt et al. 1996). Because the H_2O concentration in majoritic garnets of this study varies widely from runs conducted at similar P-T conditions, difference in chemical composition (Fe, Al, Si, and Cr content) appears to be the major cause for water content differences. Excluding the very high (80-85%) majoritic component samples (i.e., Max3 and Max4), there is generally increasing water content expressed as H atoms per formula unit (apfu) with Al^{3+} content and $Fe^{3+}/\Sigma Fe$, whereas H (apfu) increases with decreasing Fe^{2+} and Cr^{3+} (Fig. 5, Tables 3, 4). In the very high majoritic component samples, the only cation variable is Fe^{3+}, which shows a positive correlation with water content.

Nominally anhydrous majorite accommodates ‘water’ via the incorporation of hydroxyl groups. Several mechanisms are discussed for majorite, such as the hydrogarnet substitution, where silicon vacancies in the tetrahedron are charge-balanced through oxygen protonation; the substitution of silicon in the tetrahedron by trivalent aluminum and a proton; and the protonation of oxygens associated with octahedral vacancies, whereby divalent as well as trivalent cations can be involved (e.g., Rossman and Aines 1991; Hösch 1999; Bolfan-Casanova 2000; McCammon and Ross 2003; McCammon et al. 2004; Mokherjee and Karato 2010). Since tetrahedral vacancies induce an oxygen distance change from 1.63 Å in an occupied site to 1.95 Å in the vacancy (Lager and van Dreele 1996), it has been

concluded that increasing pressure will inhibit this form of substitution for garnets and therewith limits the H_2O concentration to tens of wt ppm (Bell and Rossman 1992; Withers et al. 1998).

Our IR spectra compare well with spectra of garnet and majorite reported in literature (e.g., Aines and Rossman 1984; Bell et al. 1995; Withers et al. 1998; Bolfan-Casanova et al. 2000; Katayama et al. 2003; Maldener et al. 2003). Due to their complex nature a straightforward assignment to corresponding OH incorporation mechanisms is not possible. Based on chemical composition and IR spectra we can differentiate our majoritic garnets into three different types (cf. Fig. 5, Tables 3, 4):

type I) high concentration of octahedral silicon and low to intermediate water contents, low iron, aluminum and chromium concentrations, intermediate Fe^{3+} content, weak and broad OH feature (Max3, Max4);

type II) low concentration of octahedral silicon, 0.06 to 0.10 $Fe^{3+}/\Sigma Fe$, intermediate water contents, high Al^{3+} concentration, intense OH bands at at ~3580 cm^{-1} and ~3630 cm^{-1} (MA380 – MA385), and

type III) lowest concentration of octahedral silicon, high Fe^{3+} and Al^{3+} concentrations in combination with highest water content, additional intense OH band at lower wavenumbers (MA337).

The OH bands observed in this study at ~3580 cm^{-1} and ~3630 cm^{-1} are close to the bands reportedly associated with the hydrogarnet subsititution in pyrope (Ackerman et al. 1983; Geiger 1991). However, the hydrogarnet substitution alone can not explain all OH bands in the majorite IR spectrum, additional mechanims are needed to explain the OH defect incorporation.

In a proton NMR study Cho and Rossman (1993) show that even in grossular with low water concentrations of 0.2-0.3 wt% H_2O other mechanisms than the hydrogarnet substitution are

prevailing. Andrut et al. (2002) conclude that in garnets with trace hydrogen, octahedral and dodecahedral vacancies form $SiO_3(OH)$ groups. McCammon et al. (2004) show that the oxidation of ferrous iron leads to an increased vacancy production and suggest that protonation of octahedral vacancies is the main hydration mechanism in mantle garnets. Pigott et al. (2013) further support octahedral and dodecahedral Mg vacancies to be the main protonation mechanisms in the majorite end member from atomistic simulations. Si and Mg vacancies might explain the OH features in our silicon-rich samples with near-endmember majorite composition Max3 and Max4 (type I). Positive correlations between trivalent iron and aluminum with H_2O concentration, however, lead us to conclude that in our low octahedral Si samples higher trivalent cation concentrations lead to increased vacancy production (type II samples, Fig. 5, McCammon et al. 2004). If we follow the assignment of the OH bands at ~3580 cm^{-1} and ~3630 cm^{-1} to the hydrogarnet substitution, the low band intensity in type I majorites compared to type II and type III majorites in this spectral region might be explained by the high concentration of octahedral silicon, potentially inhibiting this form of substitution and limiting the incorporation of H_2O in these samples. The additional band at lower wavenumber in water-rich type III majorite might be explained by the high Fe^{3+} concentration causing an increased vacancy production. Such vacancies might be associated with octahedral defects or Fe^{3+} substituting silicon in the tetrahedron, similar to what has been discussed for ringwoodite (Mrosko et al. 2013). However, a definite band assignment requires additional work.

The main goal of this work is to analyze the relationship between OH band position and absorption coefficient, i.e., the frequency dependence of the absorption coefficient of majoritic garnet. Figure 6 shows the general trend of absorption coefficients for water in hydrous minerals and glasses versus wavenumber of the corresponding OH bands (lines labeled 1 and 2). An increase of the coefficients with decreasing wavenumber is expected due to interrelations of OH dipole strength, O-H...O geometry and OH band intensity. For a review see Koch-Müller and Rhede (2010). However, for some minerals frequency-

independent mineral-specific absorption coefficients have been published, such as for feldspar (Johnson and Rossman 2003), rutile (Maldener et al. 2001), garnet (Hösch 1999), olivine (Thomas et al. 2009, Withers et al. 2012), wadsleyite (Deon et al. 2010) or quartz (Thomas et al. 2009). For majoritic garnet, we observe a frequency dependence of the absorption coefficient, similar to what has been communicated by Paterson (1982), Libowitzky and Rossman (1996), and for ringwoodite by Koch-Müller and Rhede (2010) (Fig. 6). From our absorption coefficients and the values of Bell et al. (1995) and Maldener et al. (2003) we calculate the following linear calibration trend based on three-dimensional absorbance data (see Fig. 6), which can be used to determine IR absorption coefficients for garnets: y= - 249x + 906128, where y is the absorption coefficient in $Lmol^{-1}cm^{-2}$ and x is the mean frequency of all OH bands in cm^{-1}.

For minerals that show a wide spectral range of OH absorption bands, such as olivine, the use of a single absorption coefficient has been suggested in the past (Thomas et al. 2009, Mosenfelder et al. 2011). Whereas Kovacs et al. (2010) propose site-specific absorption coefficients for olivine other groups see no such evidence in their studies (Koch-Müller et al. 2006; Thomas et al. 2009; Mosenfelder et al. 2011). On the contrary, e.g., Thomas et al. (2009) calculate a frequency-independent absorption coefficient for both, synthetic olivine showing group I OH bands (~3600 cm^{-1}) and olivine from Zarbargad, Egypt, with group II OH bands (3200 cm^{-1}). Based on our study the use of a single absorption coefficient for water quantification in majoritic garnet is not recommended. The need for a frequency-dependent calibration in majoritic garnet likely reflects the diversity of OH substitution mechanisms depending upon the concentration of trivalent cations and octahedrally-coordinated Si.

For majoritic garnet, we determine absorption coefficients ranging from 10470 ± 3100 $Lmol^{-1}cm^{-2}$ to 23400 ± 3100 $Lmol^{-1}cm^{-2}$. All values for our majoritic garnets are higher than the values of 6700 ± 2300 $Lmol^{-1}cm^{-2}$ reported for pyrope garnet by Bell et al. (1995) and 3630 ± 1580 $Lmol^{-1}cm^{-2}$ proposed for a series of garnets by Maldener et al. (2003), but plot below

the calibration curves of Paterson (1982) and Libowitzky and Rossman (1996). Koch-Müller et al. (2010) propose that wavenumber-independent absorption coefficients, such as those for olivine and quartz (Thomas et al. 2009), are valid for minerals having the same composition and thus comparable atomic distances. Absorption coefficients strongly depend on structure changes. This has been shown for polymorphs of SiO_2, where coefficients increase from quartz to coesite and stishovite, as the densities of the structures and thus the mean O-O distances decrease (Thomas et al., 2009; Koch-Müller and Rhede 2010). Koch-Müller and Rhede (2010) report wavenumber-dependent absorption coefficients for synthetic Fe-Mg ringwoodites, similar to what we observe for majoritic garnet. They explain this by strongly differing mineral compositions (Fe/Mg substitution), which may result in a continuous decrease of the O-H----O distances with increasing Mg. This might be also true for our set of majoritic garnets with varying chemical compositions. However, the crystal chemistry and H incorporation in majorite are too variable to confirm clear relations such as seen in the SiO_2 system or ringwoodite.

Implications

Our work illustrates that using average IR absorption values for garnet (Bell et al. 1995; Maldener et al. 2003) would lead to water content overestimation in the case of majoritic garnet, whereas the general IR calibration trends reported by Paterson (1982) and Libowitzky and Rossman (1997) would underestimate water concentrations. Our absorption coefficients give up to 4 times higher H_2O contents than these general trends would estimate, and up to 7 times lower water concentrations than the Bell et al. (1995) and Maldener et al. (2003) calibrations would imply. We have produced a linear wavenumber-dependent IR calibration for water quantification in minerals of the pyrope-majorite solid-solution series, which will result in more accurate estimations of the water content in natural and synthetic majoritic garnets. Wavenumber-dependent factors allow conversion of published H_2O concentrations that use the Paterson (1982) or Libowitzky and Rossman (1997) calibration

445 curves. For a mean wavenumber of 3550 cm^{-1}, the conversion factors are 1.54 and 2.26,
446 respectively.
447
448 **References**

449 Ackerman, L., Cemič, L., and Langer, K. (1983) Hydrogarnet substitution in pyrope: a
450 possible location for 'water' in the mantle. Earth and Planetary Science Letters, 62, 208–214.

451 Aines, R.D., and Rossman, G.R. (1984) Water content of mantle garnets, Geology,
452 12, 720–723.

453 Akaogi, M., and Akimoto, S. (1977) Pyroxene-garnet solid solution equilibria in the
454 system $Mg_4Si_4O_{12}$-$Mg_3Al_2Si_3O_{12}$ and $Fe_4Si_4O_{12}$-$Fe_3Al_2Si_3O_{12}$ at high pressures and
455 temperatures. Physics of the Earth and Planetary Interiors, 15, 90–106.

456 Amthauer, G., Annersten, H., and Hafner, S.S. (1976) The Mössbauer spectrum of
457 ^{57}Fe in silicate garnets. Zeitschrift für Kristallographie, 143, 14–55.
458
459 Anderson, D.L., and Bass, J.D. (1986) Transition region of the Earth's upper mantle,
460 Nature, 320, 321–328.
461
462 Andrut, M., Wildner, M., and Beran, A. (2002) The crystal chemistry of birefringent
463 natural uvarovites. Part IV. OH defect incorporation mechanisms in non-cubic garnets
464 derived from polarized IR spectroscopy. European Journal of Mineralogy, 14, 1019−1026.
465
466 Angel, R.J., Finger, L.W., Hazen, R.M., Kanzaki, M., Weidner, D.J., Liebermann,
467 R.C., and Veblen, D.R. (1989) Structure and twinning of single-crystal $MgSiO_3$, garnet
468 synthesized at 17 GPa and 1800°C. American Mineralogist, 74, 509-512.
469

Angel, R.J., and Finger, L.W. (2011) SINGLE: a program to control single-crystal diffractometers. Journal of Applied Crystallography, 44, 247-251.

Armstrong, J.T. (1995) CITZAF: a package of correction programs for the quantitative electron microbeam X-ray-analysis of thick polished materials, thin films, and particles. Microbeam Analysis, 4, 177–200.

Bell, D.R., and Rossman, G.R. (1992) Water in Earth's mantle: the role of nominally anhydrous minerals. Science, 255, 1391–1397.

Bell, D.R., Ihinger, P.D., and Rossman, G.R. (1995) Quantitative analysis of trace OH in garnet and pyroxenes, American Mineralogist, 80, 465–474.

Bell, D.R., Rossman, G.R., and Moore, R.O. (2004) Abundance and partitioning of OH in a high-pressure magmatic system: megacrysts from the Monastery kimberlite, South Africa. Journal of Petrology, 45, 1539-1564.

Beran, A., Langer, K., and Andrut, M. (1993) Single crystal infrared spectra in the range of OH fundamentals of paragenetic garnet, omphacite and kyanite in an eclogitic mantle xenoliths. Mineralogy and Petrology, 48, 257–268.

Beran, A., and Libowitzky, E. (2006) Water in natural mantle minerals. II: Olivine, garnet and accessory minerals. In H. Keppler and J.R. Smyth, Eds., Water in nominally anhydrous minerals, 62, p. 169-191. Reviews in Mineralogy and Geochemistry, Mineralogical Society of America, Chantilly, Virginia.

Bolfan-Casanova, N., Keppler, H., and Rubie, D.C. (2000) Water partitioning between nominally anhydrous minerals in the $MgO–SiO_2–H_2O$ system up to 24GPa: implications for

the distribution of water in the Earth's mantle. Physics of the Earth and Planetary Interiors, 182, 209–221.

Cho, H., and Rossman, G.R. (1993) Single-crystal NMR studies of low-concentration hydrous species in minerals: Grossular garnet. American Mineralogist, 78, 1149-1164.

De Grave, E., and Van Alboom, A. (1991) Evaluation of ferrous and ferric Mössbauer fractions. Physics and Chemistry of Minerals, 18, 337-342.

Deon, F., Koch-Müller, M., Rhede, D., Gottschalk, M., Wirth, R., and Thomas, S.-M. (2010): Location and quantification of hydroxyl in wadsleyite: new insights. American Mineralogist, 95, 312-322.

Gasparik, T. (2002) Experimental investigation of the origin of majoritic garnet inclusions in diamonds. Physics and Chemistry of Minerals, 29, 170-180.

Geiger, C.A., Langer, K., Bell, D.R., Rossman, G.R., and Winkler, B. (1991) The hydroxide component in synthetic pyrope. American Mineralogist, 76, 49–59.

Grove, T.L. (1981) Use of FePt alloys to eliminate the iron loss problem in 1 atmosphere gas mixing experiments: Theoretical and practical considerations. Contributions to Mineralogy and Petrology, 78, 298-304.

Hatch, D.M., and Ghose, S. (1989) Symmetry analysis of the phase transition and twinning in MgSiO garnet: Implications to mantle mineralogy, American Mineralogist, 74, 1221-1224.

Hauri, E.H., Gaetani, G.A., and Green, T.H. (2006) Partitioning of water during melting of the Earth's upper mantle at H_2O-undersaturated conditions. Earth and Planetary Science Letters, 248, 715-734.

Hazen, R.M., Downs, R.T., Conrad, P.G., Finger, L.W., and Gasparik, T. (1994) Comparative compressibilities of majorite-type garnets, Physics and Chemistry of Minerals, 21, 344–349.

Heinemann, S., Sharp, T.G., Seifert, F., and Rubie, D.C. (1997) The cubic-tetragonal phase transition in the system majorite ($Mg_4Si_4O_{12}$) - pyrope ($Mg_3Al_2Si_3O_{12}$), Physics and Chemistry of Minerals, 24, 206-221.

Hirschmann, M. (2006) Water, melting, and the deep earth H_2O cycle. The Annual Review of Earth and Planetary Science, 34, 629-653.

Hösch, A. (1999) Schwingungsspektroskopie von OH-führenden Defekten in Granat. 168 p., Ph.D. thesis, Technical University, Berlin.

Hofmeister, A.M., Giesting, P.A., Wopenka, B., Gwanmesia, G.D., and Jolliff, B.L. (2004) Vibrational spectroscopy of pyrope-majorite garnets; structural implications, American Mineralogist, 89, 132–146.

Irifune, T. (1987) An experimental investigation of the pyroxene-garnet transformation in a pyrolite composition and its bearing on the constitution of the mantle. Physics of the Earth and Planetary Interiors, 45, 324-336.

Ita, J., and Stixrude, L. (1992) Petrology, elasticity, and composition of the mantle transition zone, Journal of Geophysical Research, 97, 6849–6866.

Jeanloz, R. (1980) Majorite: vibrational and compressional properties of a high-pressure phase. Journal of Geophysical Research, 86, 6171-6179.

Johnson, E.A., and Rossman, G.R. (2003) The concentration and speciation of hydrogen in feldspars using FTIR and 1H MAS NMR spectroscopy. American Mineralogist, 88, 901-911.

Johnson, E.A. (2006) Water in nominally anhydrous crustal minerals: speciation, concentration, and geologic significance. In H. Keppler and J.R. Smyth, Eds., Water in nominally anhydrous minerals, 62, p. 117-154. Reviews in Mineralogy and Geochemistry, Mineralogical Society of America, Chantilly, Virginia.

Kanzaki, M. (1987) Ultrahigh-pressure phase relations in the system $Mg_4Si_4O_{12}$-$Mg_3Al_2Si_3O_{12}$, Physics of the Earth and Planetary Interiors, 49, 168-175.

Katayama, I., Hirose, K., Yurimoto, H., and Nakashima, S. (2003) Water solubility in majoritic garnet in subducting oceanic crust. Geophysical Research Letters, 30, 2155-2159.

Keppler, H., and Bolfan-Casanova, N. (2006) Thermodynamics of water solubility and partitioning. In H. Keppler and J.R. Smyth, Eds., Water in nominally anhydrous minerals, 62, p. 193-230. Reviews in Mineralogy and Geochemistry, Mineralogical Society of America, Chantilly, Virginia.

King, H.E., and Finger, L.W. (1979) Diffracted beam crystal centering and its application to high-pressure crystallography. Journal of Applied Crystallography, 12, 374-378.

Koch-Müller, M., and Rhede, D. (2010) IR absorption coefficients for water in

582 nominally anhydrous high-pressure minerals. American Mineralogist, 95, 770 – 775.
583
584 Koch-Müller, M., Matsyuk, S.S., Rhede, D., Wirth, R., and Khisina, N. (2006) Hydroxyl
585 in mantle olivine xenocrysts from the Udachnaya kimberlite pipe. Physics and Chemistry of
586 Minerals, 33, 276–287.
587
588 Koga, K., Hauri, E., Hirschmann, M., and Bell, D. (2003) Hydrogen concentration
589 analyses using SIMS and FTIR: comparison and calibration for nominally anhydrous
590 minerals. Geochemistry, Geophysics, Geosystems, 4(2).
591
592 Kohlstedt, D.L., Keppler, H., and Rubie, D.C. (1996) Solubility of water in the α, β and
593 γ phases of $(Mg,Fe)_2SiO_4$, Contributions to Mineralogy and Petrology, 123, 345–357.
594
595 Lager, G.A., and Von Dreele, R.B. (1996) Neutron powder diffraction study of
596 hydrogarnet to 9.0 GPa. American Mineralogist, 81, 1097–1104.
597
598 Lenz, S. (2012): Synthese und Charakterisierung von Majorit, 380 p. B.S. thesis, TU
599 Berlin, Germany.
600
601 Libowitzky, E., and Rossman, G.R. (1996) Principles of quantitative absorbance
602 measurements in anisotropic crystals. Physics and Chemistry of Minerals 23, 319-327.
603
604 Libowitzky, E., and Rossman, G.R. (1997) An IR absorption calibration for water in
605 minerals. American Mineralogist, 82, 1111-1115.
606
607 Lu, R., and Keppler, H. (1997) Water solubility in pyrope to 100 kbar, Contributions to
608 Mineralogy and Petrology, 129, 35-42.

Maldener, J., Rauch, F., Gavranic, M., and Beran, A. (2001) OH absorption coefficients of rutile and cassiterite deduced from nuclear reaction analysis and FTIR spectroscopy. Mineralogy and Petrology, 71, 21-29.

Maldener, J., Hösch, A., Langer, K., and Rauch, F. (2003) Hydrogen in some natural garnets studied by nuclear reaction analysis and vibrational spectroscopy. Physics and Chemistry of Minerals, 30, 337–344.

McCammon, C.A., and Ross, N.L. (2003) Crystal chemistry of ferric iron in (Mg, Fe)(Si,Al)O_3 majorite with implications for the transition zone. Physics and Chemistry of Minerals, 30, 206–216.

McCammon, C.A., Frost, D.J., Smyth, J.R., Laustsen, H.M.S., Kawamoto, T., Ross, N.L., and van Aken, P.A. (2004) Oxidation state of iron in hydrous mantle phases: implications for subduction and mantle oxygen fugacity. Physics of the Earth and Planetary Interiors, 143-144, 157-169.

McMillan, P., Akaogi, M., Ohtani, E., Williams, Q., Nieman, R., and Sato, R. (1989) Cation disorder in garnets along the Mg3Al2Si3O12-Mg4Si4O12 join: An infrared, Raman and NMR study. Physics and Chemistry of Minerals, 16, 428–435.

Mookherjee, M., and Karato, S. (2010) Solubility of water in pyrope-rich garnet at high pressures and temperature. Geophysical Research Letters, 37, L03310.

Moore, R.O., and Gurney, J.J. (1985) Pyroxene solid solution in garnets included in diamond. Nature, 318, 553-555.

Mosenfelder, J.L, Le Voyer, M., Rossman, G.R., Guan, Y., Bell, D.R., Asimow, P.D., and Eiler, J.M. (2011) Analysis of hydrogen in olivine by SIMS: Evaluation of standards and protocol. American Mineralogist, 96, 1725-1741.

Mrosko, M., Koch-Müller, M., and Schade, U. (2011) In-situ mid/far micro-FTIR spectroscopy to trace pressure-induced phase transitions in strontium feldspar and wadsleyite. American Mineralogist, 96, 1748–1759.

Mrosko, M., Lenz, S., McCammon, C.A., Taran, M., Wirth, R., and Koch-Müller, M. (2013) Hydrogen incorporation and the oxidation state of iron in ringwoodite: A spectroscopic study. American Mineralogist, 98, 629-636.

Murakami, M., Sinogeikin, S. V., Litasov, K., Ohtani, E., Bass, J.D. (2008) Single-crystal elasticity of iron-bearing majorite to 26 GPa: Implications for the seismic velocity structure of the mantle transition zone, Earth and Planetary Science Letters, 274, 339-345.

Paterson, M.S. (1982) The determination of hydroxyl by infrared absorption in quartz, silicate glass and similar materials, Bulletin de Mineralogie, 105, 20–29.

Pawley, A.R., McMillan, P.F., and Holloway, J.R. (1993) Hydrogen in stishovite, with implications for mantle water content, Science, 261, 1024–1026.

Pearson, D.G., Brenker, F.E., Nestola, F., McNeill, J., Nasdala, L., Hutchison, M.T., Matveev, S., Mather, K., Silversmit, G., Schmitz, S., Vekemans, B., and Vincze, L. (2014) Hydrous mantle transition zone indicated by ringwoodite included within diamond. Nature, 507, 221–224.

Pigott, J.S., Wright, K., Gale, J.D., and Panero, W.R. (2013) Calculation of the Energetics of Water Incorporation in Majorite Garnet. Transactions of the American Geophysical Union, 93, Fall Meeting Supplement, San Francisco.

Prescher, C., McCammon, C., and Dubrovinsky, L. (2012) MossA - a program for analyzing energy-domain Mossbauer spectra from conventional and synchrotron sources. Journal of Applied Crystallography, 45, 329-331.

Ringwood, A.E. (1967) The pyroxene-garnet transformation in the Earth's mantle. Earth and Planetary Science Letters, 2, 255-263.

Ringwood, A.E., and Major, A. (1967) Some high-pressure transformations of geophysical significance, Earth and Planetary Science Letters, 2, 106.

Ringwood, A.E., and Major, A. (1971) Synthesis of majorite and other high-pressure garnet. Earth and Planetary Science Letters, 12, 411-418.

Rossman, G.R. (1988) Vibrational spectroscopy of hydrous components. In F.C. Hawthorne, Ed., Spectroscopic methods in mineralogy and geology 18, p. 193-206, Reviews in Mineralogy, Mineralogical Society of America, Washington, D.C.

Rossman, G.R., Rauch, F., Livi, R., Tombrello, T.A., Shi, C.R., and Zhou, Z.Y. (1988) Nuclear reaction analysis of hydrogen in almandine, pyrope, and spessartine garnets. Neues Jahrbuch für Mineralogie Monatshefte, 4, 172-178.

Rossman, G.R. (1990) Hydrogen in “anhydrous” minerals. Nuclear Instruments and Methods in Physics Research, B45, 41-44.

Rossman, G.R., and Aines, R.D. (1991) The hydrous components in garnets: grossular-hydrogrossular. American Mineralogist 76, 1153-1164.

Schmandt, B., Jacobsen, S.D., Becket, T.W., Liu, Z., and Dueker, K.G. (2014) Dehydration melting at the top of the lower mantle. Science, 344, 1265-1268.

Schmidt, M.W., and Ulmer, P. (2004) A rocking multianvil: Elimination of chemical segregation in fluid-saturated high-pressure experiments. Geochimica et Cosmochimica Acta, 68, 1889-1899.

Smith, J.V., and Mason, B. (1970) Pyroxene-garnet transformation in Coorara meteorite. Science, 168, 832-833.

Smyth, J.R., and Jacobsen, S.D. (2006) Nominally Anhydrous Minerals and Earth's Deep Water Cycle. *In:* Earth's Deep Water Cycle, Jacobsen, S.D. and van der Lee (Eds.) American Geophysical Union, Geophysical Monograph Series 168, 1-11.

Stern, C.R., Kilian, R., Olker, B., Hauri, E.H., and Kurtis Kyser, E. (1999) Evidence from mantle xenoliths for relatively thin (<100 km) continental lithosphere below the Phanerozoic crust of southernmost South America. Lithos, 48, 217-235.

Thomas, S.-M., Thomas, R., Davidson, P., Reichart, P., Koch-Müller, M. Dollinger, G. (2008) Application of Raman spectroscopy to quantify trace water concentrations in glasses and garnets. American Mineralogist, 93, 1550-1557.

Thomas, S.-M., Koch-Müller, M., Reichart, P., Rhede, D., Thomas, R., Wirth, R., Matsyuk, S. (2009) IR calibrations for water determination in olivine, r-GeO_2 and SiO_2-polymorphs. Physics and Chemistry of Minerals, 36, 489-509.

Withers, A.C., Wood, B.J, and Carroll, M.R. (1998) The OH content of pyrope at high pressure, Chemical Geology, 147, 161–171.

Withers, A.C., Bureau, H., Raepsaet, C., and Hirschmann, M.M. (2012) Calibration of infrared spectroscopy by elastic recoil detection analysis of H in synthetic olivine. Chemical Geology, 334, 92-98.

Acknowledgements

SMT thanks Rainer Thomas for discussions, and Andreas Ebert (GFZ Potsdam) and Dan Frost (BGI) for help with the syntheses. This research was supported by NSF grant EAR-1215957 awarded to SMT and by grants from the NSF (EAR-0748707), the David & Lucile Packard Foundation, and the Carnegie/DOE Alliance Center (CDAC) to SDJ.

Figure Captions

Fig. 1 Room temperature Mössbauer spectra of samples (a) MA380, (b) MA382, (c) MA384, (d) MA385, (e) Max3, and (f) Max4. The doublets assigned to dodecahedral Fe^{2+}, octahedral Fe^{3+}, and octahedral Fe^{2+} are shaded white, light grey and dark grey, respectively. The residuals of the fits are shown above each spectrum and the velocity scale is relative to α-Fe.

Fig. 2 Unpolarized IR spectra of majoritic garnet at room conditions. Spectra are offset for clarity. Spectral information and sample thicknesses are given in Table 4.

Fig. 3 Raman spectra of MA384 (black) and Max4 (red) showing characteristic lattice vibrations in the low-frequency range.

Peak positions are slightly shifted depending on the silicon content.

Fig. 4 Unpolarized Raman spectra of MA337 (upper, free-standing single-crystal) and MA380 (lower, thin section) showing OH bands in the high-frequency range agree well with IR spectra. Integrated intensities were used for quantitative OH analyses. The additional band at ~ 3050 cm^{-1} in the spectrum of MA380 (lower) is due to C-H stretching of the oxirane group of epoxy resin and was excluded from calculations.

Fig. 5 Comparison between H (apfu) Si and chemical sample composition. We observe a positive linear correlation between the water concentration of the samples and the integrated OH band area from IR spectroscopy. In addition, positive correlations between sample water content and trivalent cations Fe^{3+} and $Al^{3+}$are illustrated here. Sample water content and Cr^{3+} are negatively correlated. Note however, that this relationship seems to hold only for samples with lower concentrations of octahedral silicon (i.e., smaller majorite component) and higher concentrations of trivalent cations (see Tables 3, 4).

Fig. 6 Comparison of mineral-specific IR absorption coefficients calculated in this study and data from 1) Paterson (1982), 2) Libowitzky and Rossman (1997), 3) Bell et al. 1995, and 4) Maldener et al. (2003). The x-axis gives mean wavenumbers of all OH bands calculated from peak fitting. Great care must be taken when comparing published absorption coefficients. This figure contains values derived from one absorbance direction multiplied by three to allow comparison between published absorption coefficient values. Some authors such as Paterson (1982) and Libowitzky and Rossman (1997) use the sum of absorbances (total absorbance) in all three orthogonal directions of a crystal to calculate the absorption coefficient, whereas others such as Bell et al. (1995) and Maldener et al. (2003) use only one-directional information. The linear regression (dashed line), y=-249x + 906128 (R^2=0.63571), allows calculation of IR absorption coefficients for water quantification in garnets.

Table 1. Starting compositions and experimental conditions. Samples, to which water was added, are marked by footnotes.

Run no.	P(GPa)	T (°C)	Starting composition
MA380	18	1800	$(Mg_2Fe_1)(Si_{0.2}Mg_{0.2}Al_{1.4}Cr_{0.2})[SiO_4]_3$
MA382	18	1800	$(Mg_{1.8}Fe_{1.5})(Si_{0.2}Mg_{0.2}Al_{1.4}Cr_{0.2})[SiO_4]_3$
MA384#	18	1800	$(Mg_2Fe_1)(Al_{1.9}Cr_{0.1})[SiO_4]_3$
MA385#	18	1800	$(Mg_2Fe_1)(Si_{0.2}Mg_{0.2}Al_{1.4}Cr_{0.2})[SiO_4]_3$
MA337*	18	1500	$(Mg_2Fe_1)(Al_{1.9}Cr_{0.1})[SiO_4]_3$
Max3&	19	1800	orthopyroxene (En^{90})
Max4&	19	1800	orthopyroxene (En^{90})

Note that starting materials of samples MA380, MA382, MA384 and MA385 were placed in Fe-doped Pt-capsules to reduce the potential loss of Fe during synthesis (see Grove et al., 1981).
#0.5 µl bidistilled H_2O was added.
**2 µl bisdistilled H_2O was added.*
&Starting material was a natural orthopyroxene from garnet-peridot sample TM-17 from the study of Stern et al. (1999). H_2O was added as brucite.

Table 2. Lattice parameters of majoritic garnets in this study.

	Unconstrained Least Squares	Constrained Least Squares (Cubic)

Sample	a (Å)	b (Å)	c (Å)	a (Å)	Volume (Å^3)
MA380	11.4870(2)	11.4873(2)	11.4774(2)	11.48710(9)	1515.76(4)
MA382	11.4827(2)	11.4833(4)	11.4829(4)	11.4830(2)	1514.14(7)
MA384	11.4795(3)	11.4794(3)	11.4796(3)	11.4795(2)	1512.76(6)
MA385	11.4853(2)	11.4855(2)	11.4856(2)	11.48546(9)	1515.12(3)
MAX3	11.4966(2)	11.4966(2)	11.4968(2)	11.49673(9)	1519.58(4)
MAX4	11.501(1)	11.513(1)	11.504(1)	11.5061(8)	1523.3(3)
MA337*	-	-	-	11.4825(3)	1513.94(2)

*Data from Lenz (2012).

Table 3. Composition of majoritic garnets determined by electron microprobe analyses and Mössbauer spectroscopy.

Run no.	Oxides (wt%)						Mineral formula (based on 12 Oxygens)[$]	$Fe^{3+}/\Sigma Fe$
	MgO	FeO	SiO_2	Al_2O_3	Cr_2O_3	Total		
MA380	21.41(71)	13.65(131)	43.22(40)	18.73(14)	3.00(05)	100.18	$(Mg_{2.3}Fe^{2+}_{0.79})(Si_{0.11}Al_{1.59}Cr_{0.17}Fe^{3+}_{0.03})[SiO_4]_3$	0.09 ± 0.04
MA382	16.08(24)	20.88(44)	40.99(14)	18.34(17)	3.34(10)	99.64	$(Mg_{1.80}Fe^{2+}_{1.27})(Si_{0.08}Al_{1.62}Cr_{0.2}Fe^{3+}_{0.03})[SiO_4]_3$	0.06 ± 0.02
MA384	23.53(42)	10.22(84)	42.92(28)	20.98(61)	1.47(04)	99.20	$(Mg_{2.50}Fe^{2+}_{0.59})(Si_{0.06}Al_{1.76}Cr_{0.08}Fe^{3+}_{0.02})[SiO_4]_3$	0.09 ± 0.03
MA385	22.96(26)	11.61(35)	42.92(29)	20.04(14)	2.08(13)	99.64	$(Mg_{2.45}Fe^{2+}_{0.66})(Si_{0.07}Al_{1.69}Cr_{0.12}Fe^{3+}_{0.03})[SiO_4]_3$	0.10 ± 0.03
MA337	20.78(48)	13.14(90)	42.32(44)	21.41(50)	1.60 (18)	99.25	$(Mg_{2.23}Fe^{2+}_{0.72})(Si_{0.05}Al_{1.82}Cr_{0.09}Fe^{3+}_{0.07})[SiO_4]_3$	0.21 ± 0.04[#]
Max3	34.26(23)	4.23(29)	54.87(28)	4.82(38)	0.54(05)	99.25	$(Mg_{2.74}Fe^{2+}_{0.23}Ca_{0.04})(Si_{0.79}Mg_{0.79}Al_{0.39}Cr_{0.03}Fe^{3+}_{0.01})[SiO_4]_3$	0.12 ± 0.03
Max4	33.86(45)	5.03(17)	55.03(54)	4.31(21)	0.52(03)	99.43	$(Mg_{2.68}Fe^{2+}_{0.27}Ca_{0.05})(Si_{0.82}Mg_{0.82}Al_{0.35}Cr_{0.03}Fe^{3+}_{0.02})[SiO_4]_3$	0.17 ± 0.03

*Numbers in parentheses give 1σ standard deviation in terms of the preceding figure.
[#]Determined with EELS (cf. Lenz 2012).
[$]Note that the mineral formula is based on a coupled substitution with octahedrally coordinated fourvalent silicon and one divalent cation in equal amounts replacing two trivalent cations (Ringwood 1967; Ringwood and Major 1971), which is not shown here to simplify matters.

Table 4. IR spectroscopic data for H_2O analyses.

Run no.	Sample thickness (µm)	Density (g/cm^3)	Molar volume (cm^3)	OH band positions (cm^{-1})					A_i(cm^{-1})	Mean wavenumber (cm^{-1})	Independent determined water content from SIMS (wt ppm)	H /10^6 Si	H (apfu)	Absorption coefficient (L/(mol$_{H2O}$cm^2)
MA380	40	3.79	114.10	3295	3430	3526	3582	-	7.46	3442	500 ± 35 / (440 ± 60*)	7999 ± 560	0.024(2)	17720 ± 1800
MA382	30	3.94	113.98	-	3395	3545	3592	-	2.18	3475	214 ± 15	3567 ± 250	0.011(1)	15530 ± 1600
MA384	40	3.72	113.87	3206	3441	-	3606	3637	14.70	3474	881 ± 62	13927 ± 975	0.042(3)	20130 ± 2000
MA385	40	3.75	114.05	3184	3467	-	3580	3620	6.27	3483	665 ± 47	10572 ± 740	0.032(2)	11310 ± 1100
MA337*	45	3.77	113.96	3127	3412	3526	3577	3632	21.7	3450	2200 ± 500*	35052 ± 8062	0.105(24)	10470 ± 3100[#]
Max3	40	3.58	114.39	3245	3472	-	-	-	2.35	3359	126 ± 9	1930 ± 135	0.006(04)	23400 ± 2300
Max4	35	3.59	114.67	3291		3512		3620	6.5	3414	711 ± 50	10897 ± 763	0.033(2)	13090 ± 1300

*Water content determined with Raman spectroscopy (cf. methods section).
[#]The IR absorption coefficient error reflects the standard deviation of integrated absorbance values, which might be due to contamination with molecular water (cf. Lenz 2012).
[$]Note that some authors such as Paterson (1982) and Libowitzky and Rossman (1997) use the sum of absorbances (total absorbance) in all three orthogonal directions of a crystal to calculate the absorption coefficient, others such as Bell et al. (1995) and Maldener et al. (2003) use only one-directional information. Here, we use values derived from one absorbance direction to allow comparison between published absorption coefficient values.

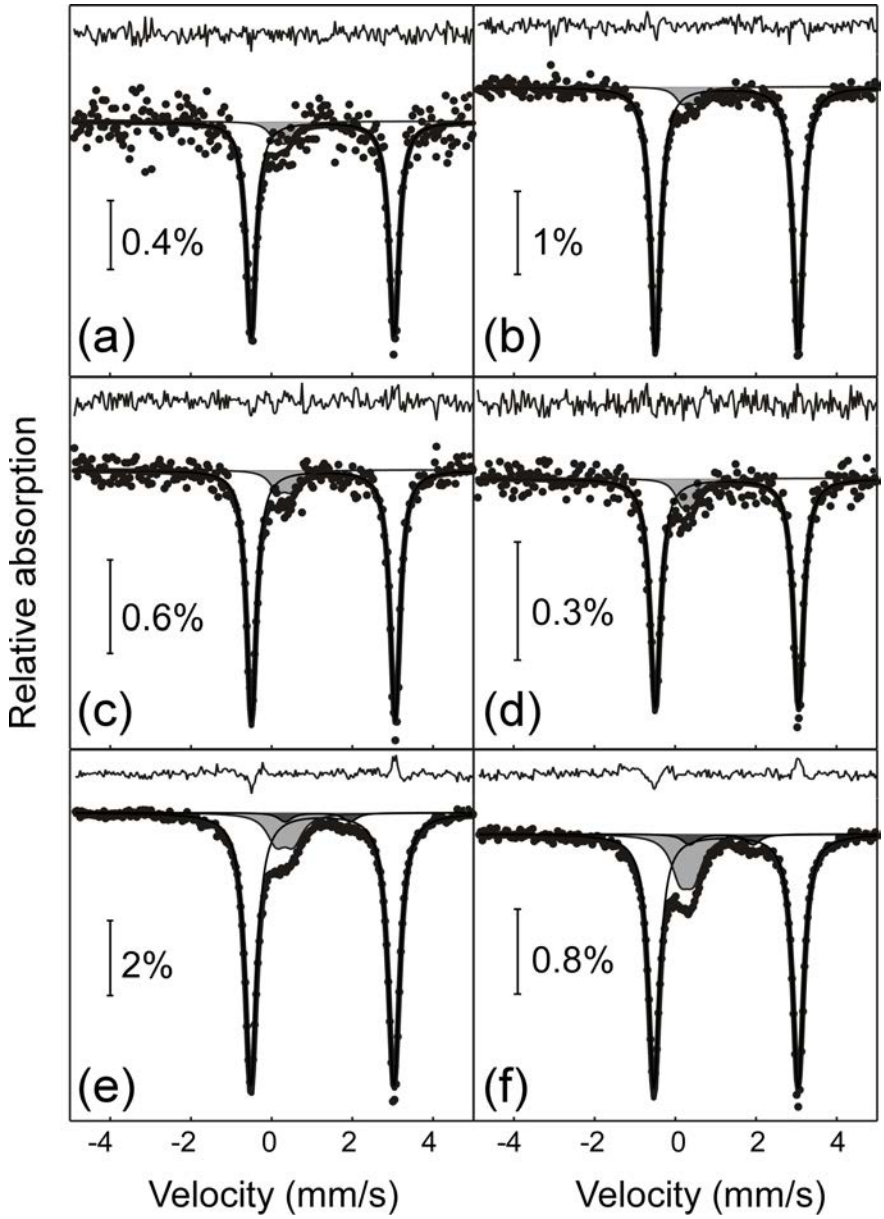

Fig. 1 Room temperature Mössbauer spectra of samples (a) MA380, (b) MA382, (c) MA384, (d) MA385, (e) Max3, and (f) Max4. The doublets assigned to dodecahedral Fe^{2+}, octahedral Fe^{3+}, and octahedral Fe^{2+} are shaded white, light grey and dark grey, respectively. The residuals of the fits are shown above each spectrum and the velocity scale is relative to α-Fe.

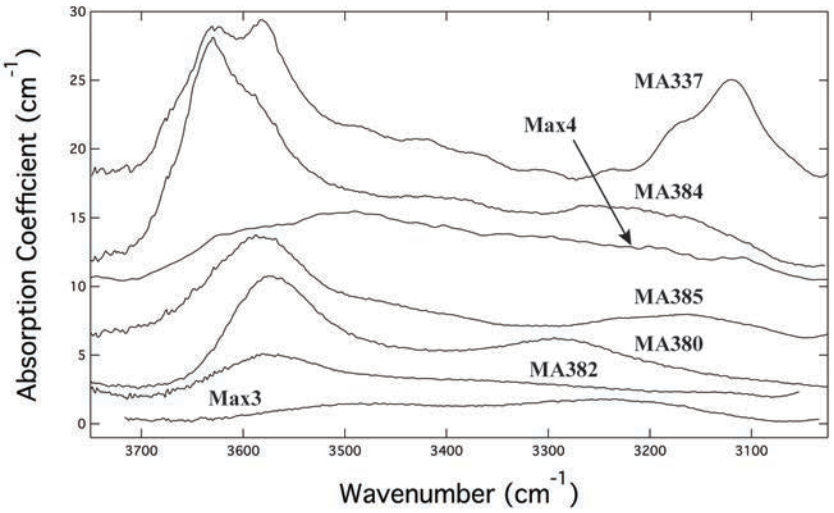

Fig. 2 Unpolarized IR spectra of majoritic garnet at room conditions. Spectra are offset for clarity. Spectral information and sample thicknesses are given in Table 4.

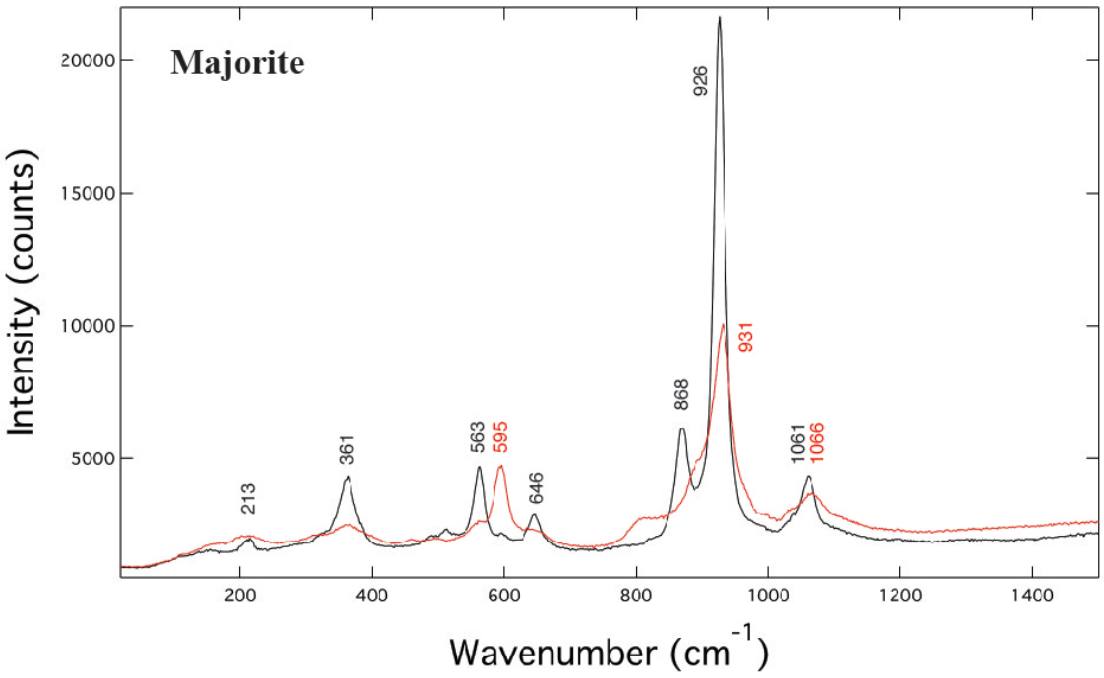

Fig. 3 Raman spectra of MA384 (black) and Max4 (red) showing characteristic lattice vibrations in the low-frequency range. Peak positions are slightly shifted depending on the silicon content.

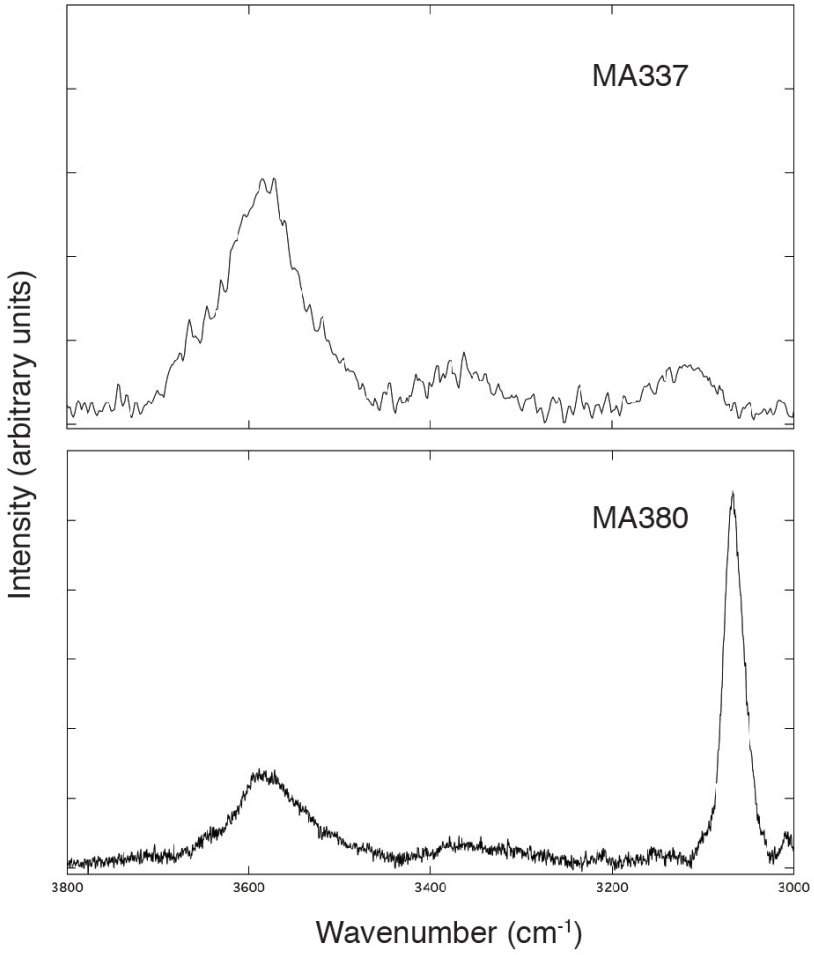

Fig. 4 Unpolarized Raman spectra of MA337 (upper, free-standing single-crystal) and MA380 (lower, thin section) showing OH bands in the high-frequency range agree well with IR spectra. Integrated intensities were used for quantitative OH analyses. The additional band at ~ 3050 cm^{-1} in the spectrum of MA380 (lower) is due to C-H stretching of the oxirane group of epoxy resin and was excluded from calculations.

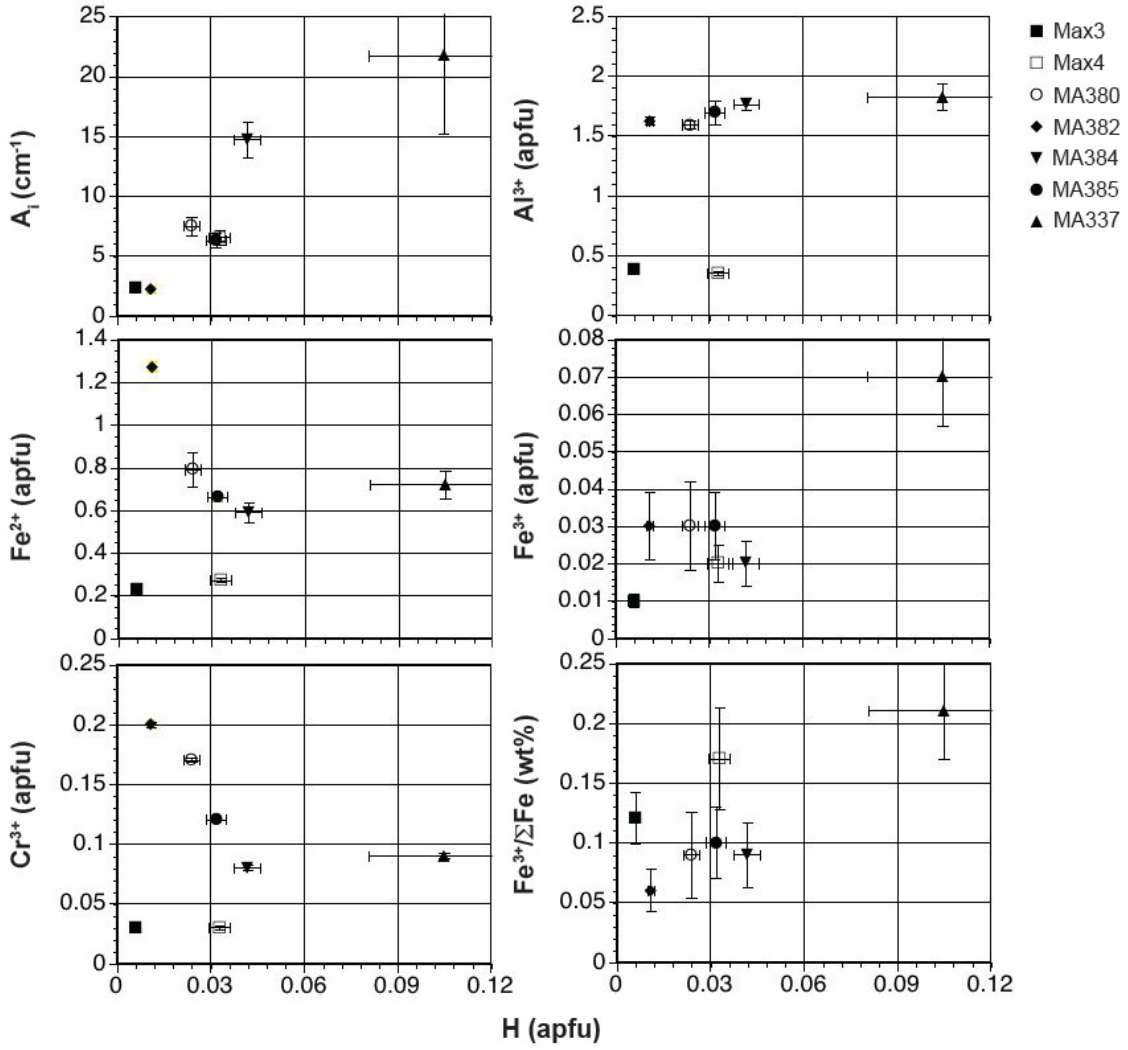

Fig. 5 Comparison between H (apfu) Si and chemical sample composition. We observe a positive linear correlation between the water concentration of the samples and the integrated OH band area from IR spectroscopy. In addition, positive correlations between sample water content and trivalent cations Fe^{3+} and $Al^{3+}$are illustrated here. Sample water content and Cr^{3+} are negatively correlated. Note however, that this relationship seems to hold only for samples with lower concentrations of octahedral silicon (i.e., smaller majorite component) and higher concentrations of trivalent cations (see Tables 3, 4).

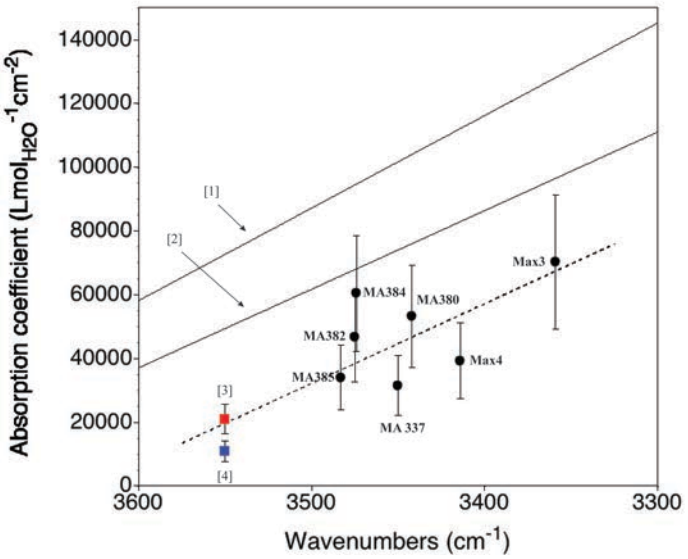

Fig. 6 Comparison of mineral-specific IR absorption coefficients calculated in this study and data from 1) Paterson (1982), 2) Libowitzky and Rossman (1997), 3) Bell et al. 1995, and 4) Maldener et al. (2003). The x-axis gives mean wavenumbers of all OH bands calculated from peak fitting. Great care must be taken when comparing published absorption coefficients. This figure contains values derived from one absorbance direction multiplied by three to allow comparison between published absorption coefficient values. Some authors such as Paterson (1982) and Libowitzky and Rossman (1997) use the sum of absorbances (total absorbance) in all three orthogonal directions of a crystal to calculate the absorption coefficient, whereas others such as Bell et al. (1995) and Maldener et al. (2003) use only one-directional information. The linear regression (dashed line), y=-249x + 906128 (R^2=0.63571), allows calculation of IR absorption coefficients for water quantification in garnets.